

Decentralized Power Allocation for MIMO-NOMA Vehicular Edge Computing Based on Deep Reinforcement Learning

Hongbiao Zhu, Qiong Wu, *Member, IEEE*, Xiaojun Wu, *Member, IEEE*, Qiang Fan,
Pingyi Fan, *Senior Member, IEEE*, Jiangzhou Wang, *Fellow, IEEE*

Abstract

Vehicular edge computing (VEC) is envisioned as a promising approach to process the explosive computation tasks of vehicular user (VU). In the VEC system, each VU allocates power to process partial tasks through offloading and the remaining tasks through local execution. During the offloading, each VU adopts the multi-input multi-out and non-orthogonal multiple access (MIMO-NOMA) channel to improve the channel spectrum efficiency and capacity. However, the channel condition is uncertain due to the channel interference among VUs caused by the MIMO-NOMA channel and the time-varying path-loss caused by the mobility of each VU. In addition, the task arrival of each VU is stochastic in the real world. The stochastic task arrival and uncertain channel condition affect greatly on the power consumption and latency of tasks for each VU. It is critical to design an optimal power allocation scheme considering the stochastic task arrival and channel variation to optimize the long-term reward including the power consumption and latency in the MIMO-NOMA VEC. Different from the traditional centralized deep reinforcement learning (DRL)-based scheme, this paper constructs a decentralized DRL framework to formulate the power allocation optimization problem, where the local observations are selected as the state. The deep deterministic policy gradient (DDPG) algorithm is adopted to learn the optimal power

Hongbiao Zhu and Qiong Wu are with the School of Internet of Things Engineering, Jiangnan University, Wuxi 214122, China (e-mail: hongbiaozhu@stu.jiangnan.edu.cn, qiongwu@jiangnan.edu.cn).

Xiaojun Wu is with the School AI & CS, Jiangnan University, Wuxi 214122, China (wu_xiaojun@jiangnan.edu.cn).

Qiang Fan is with Wistron AiEdge, San Jose, CA 95131, USA (e-mail: qiang_fan@wistron.com).

Pingyi Fan is with the Department of Electronic Engineering, Beijing National Research Center for Information Science and Technology, Tsinghua University, Beijing 100084, China (email: fpy@tsinghua.edu.cn).

Jiangzhou Wang is with the School of Engineering and Digital Arts, University of Kent, CT2 7NT Canterbury, U.K. (Email: j.z.wang@kent.ac.uk).

allocation scheme based on the decentralized DRL framework. Simulation results demonstrate that our proposed power allocation scheme outperforms the existing schemes.

Index Terms

power allocation, vehicular edge computing, deep reinforcement learning, decentralized

I. INTRODUCTION

With the increasing number of vehicles, the growing demand of computation-intensive applications such as virtual/augmented reality (VR/AR), image processing, face detection and recognition is emerging to satisfy the infotainment experience of vehicular users (VUs) [1]. These applications are realized through collecting a great amount of data by various vehicular user equipments such as smart phones and wearable devices. Such large amount of data results in intensive computation tasks which need to be processed in time, thus leading to heavy computation burden for VUs [2], [3]. Vehicular edge computing (VEC) is a promising way to relieve the burden, where a VEC server with high computational capability is connected with a base station (BS) to provide VUs with computation resources at the edge [4]. When a VU has some tasks to process, it can either offload the tasks to the VEC server collocated with the BS [5], or execute the tasks locally. For the task offloading, the VU has to consume energy in the data transmission, where the offloading power is defined as the transmission power. In addition, when the VU processes the tasks locally, the local task processing will incur the energy consumption at its central processing unit (CPU). For simplicity, we define the power consumption of task processing at the VU as the local execution power.

During the offloading, the multi-input multi-out and non-orthogonal multiple access (MIMO-NOMA) channel is considered here due to its high channel spectrum efficiency and channel capacity. Specifically, each VU can share the whole spectrum and undivided bandwidth to offload tasks and the BS is equipped with multi-antenna to receive tasks from all VUs simultaneously [6]–[9]. However, the channel condition is time varying due to the channel interference among VUs caused by the MIMO-NOMA channel and the time-varying path-loss caused by the mobility of each VU. In addition, the task arrival of each VU is stochastic in practice. The stochastic task arrival and uncertainty of channel condition significantly impact the power consumption and latency of task processing for each VU. For example, a VU would take more time in task offloading when task arrival rate is increasing and the channel condition is getting deteriorated, which increases the power consumption and latency. In this case, the VU should allocate more local execution power to reduce the power consumption and latency. In the VEC, vehicular user equipments have limited energy and the applications such as virtual/augmented reality (VR/AR) and

real-time interactive 3D gaming should be processed within a limited time, therefore power consumption and latency are two important performance metrics in task processing [10], [11]. It is critical to design an optimal power allocation scheme considering the stochastic task arrival and uncertainty of channel condition in the MIMO-NOMA VEC.

Deep reinforcement learning (DRL) is a favorable framework to formulate the similar optimization problem in complex environments [12]. Many existing works have designed the offloading scheme based on the centralized DRL framework in VEC by taking various factors into account, where the BS first collects the global information including all VUs' states to determine the action of each VU, which causes huge overhead and extra latency [13]–[24]. Only a few works focused on decentralized DRL-based offloading schemes, where each VU collects the local observations to select its action, thus the overhead and latency can be reduced efficiently [25], [26]. However, these works did not consider the channel caused by employing the MIMO-NOMA mode. To the best of our knowledge, no work has considered the stochastic task arrival and the uncertainty of MIMO-NOMA channel condition in the decentralized DRL-based optimal power allocation scheme in VEC.

In this paper, we consider the stochastic task arrival, and the channel condition uncertainty caused by the MIMO-NOMA channel interference and the mobility of VUs, and propose a decentralized DRL-based power allocation scheme to optimize the long-term reward in VEC in terms of power consumption and latency. The main contributions of this paper are summarized as follows.

- 1) We formulate the power allocation optimization problem, where the state, action and reward function are elaborately defined to enable each VU to learn optimal power allocation scheme according to the local observations. Then, the deep deterministic policy gradient (DDPG) algorithm is adopted to learn the optimal power allocation decision based on the DRL framework.
- 2) Extensive experiments are carried out to test the performance of the proposed scheme and show its superiority to other existing policies in terms of power consumption and latency of task processing.

The rest of the paper is organized as follows. Section II reviews the related work. Section III introduces the system model. In Section IV the decentralized DRL framework is set up to formulate the power allocation problem. Section V presents the DDPG algorithm on how to learn the optimal power allocation scheme based on the DRL framework. Section VI presents the simulation results. It is concluded in Section VII.

II. RELATED WORK

In this section, we first review the related works on the offloading scheme in mobile edge computing (MEC) considering the MIMO or NOMA channel, then we review the existing works on the DRL-based

offloading scheme in the VEC.

A. Offloading in MIMO or NOMA MEC

In recent years, many works have considered the MIMO or NOMA channel while designing the offloading scheme in MEC.

In [27], Wang *et al.* employed NOMA channel in MEC computation offloading system to minimize the energy consumption of all users where Lagrange dual was adopted to make decisions about task offloading proportion, successive interference cancellation order, offloading power and local CPU frequencies. In [28], Pan *et al.* considered NOMA channel in MEC for uploading computation tasks and downloading computation result where convex optimization was adopted to minimize the energy consumption by determining offloading task partitions, offloading power and task time allocation. In [29], Huang *et al.* focused on the channel estimation process with pilots in massive MIMO MEC system to minimize the offloading latency of all users by optimizing power of pilot transmission and data transmission, as well as the allocation of computing resource. In [30], Ding *et al.* studied a multi-user MIMO (MU-MIMO) MEC system to minimize the system cost, the weighted sum of latency and energy consumption. In [31], Feng *et al.* considered the fairness of all users in a MU-MIMO MEC system and to minimize offloading latency through optimizing the distribution of resource, transmission of pilot sequence and data. However, these works did not consider the scenario of vehicular scenarios.

B. DRL-based Offloading in VEC

Many works have discussed DRL-based offloading scheme in VEC. In [16], Dong *et al.* considered NOMA channel in VEC where Deep Q-Network (DQN) was applied to guarantee the delay requirement and minimize the energy consumption. In [17], Ke *et al.* designed a three-layer VEC offloading system including a macro BS, multiple small BSs and vehicles where DRL is applied to minimize the cost consisting of energy consumption and transmission delay. In [18], He *et al.* proposed an offloading scheme considering network, cache, and computation resource in VEC, where DQN was employed to select the optimal offloading decision that maximizes the reward including the caching state, computation capability and received signal-to-noise ratio (SNR). In [19], Tan *et al.* formulated the joint optimal caching and computing allocation problem to minimize the VEC system cost including communication, computation and storage under the constraint of server deadline. DQN was employed to solve the optimization problem where the channel was assigned by orthogonal frequency division multiplexing (OFDM). In [20], Ning *et al.* constructed an edge computation and cache model for VEC consisting of macro BS, several RSUs and VUs, where the tasks of VUs were divided into computing tasks and content tasks. DDPG was employed

to obtain the optimal resource allocation in order to maximize the reward of mobile network operator (MNO), including computing and caching cost, penalty on quality of experience (QoE). In [21], Liu *et al.* took stochastic traffic and uncertain communication conditions of VEC into consideration, and adopted the semi-Markov process to formulate an optimization problem to maximize the total network utility of the VEC. The DQN method was employed to obtain the optimal offloading scheme. In [24], Ren *et al.* designed a VEC architecture consisting of BSs, RSUs, VUs, and cell software designed network controller where tasks can be migrated among BSs and RSUs. A centralized DRL-based offloading scheme was designed to manage the network resource through making decisions of offloading, migration and resource allocation. However, these works only focused on the centralized DRL-based offloading scheme.

A few works have also focused on decentralized DRL-based offloading schemes in VEC [25], [26]. In [25], Ye *et al.* considered a VEC that is composed of vehicle-to-vehicle (V2V) and vehicle-to-infrastructure (V2I) communications where V2I communication reserved orthogonal single-input single-output (SISO) channels. DQN was adopted to select the task transmitting sub-band and power level for VUs to maximize the reward consisting of system communication capacity and latency. In [26], Xu *et al.* considered the similar scenario [25] to maximize the sum-rate of every sub-band communication where DDPG was employed to obtain the optimal policy in continuous action space. However, [25], [26] did not consider the channel varying caused by the MIMO-NOMA channel interference and the mobility of VU in VEC.

As mentioned above, no work has considered the stochastic task arrival and channel varying in the MIMO-NOMA VEC while designing the decentralized DRL-based power allocation scheme.

III. SYSTEM MODEL

The system model is shown as Fig. 1. Consider a VEC system where an N -antenna BS is placed along a one-way J -lane road and a VEC server is attached to the BS. The lanes from near to far according to the vertical distance to the BS are denoted as $1, 2, \dots, j, \dots, J$, respectively. M vehicles on different lanes traverse the coverage of BS from left to right with different velocities, where each vehicle carries a computation resource-limited single-antenna VU. The duration time that a VU on lane j stays in the transmission coverage of BS is divided into N_j equal time slots, each of which is a constant τ_0 . At each slot, computation-intensive tasks arrive at the first come first service (FCFS) buffer of each VU stochastically following independent and identical distribution (i.i.d.). Meanwhile, each VU allocates the local execution power and offloading power to process the tasks stored in the buffer queue locally or at the VEC server nearby, respectively. Moreover, the channel condition varies due to the interference among VUs' MIMO-NOMA channel and the time-varying path-loss caused by the mobility of VUs. During the

TABLE I: The summary for notations.

Notation	Description	Notation	Description
$a_m(t)$	Task bits of user m arrived at slot t .	$a_{m,t}$	Action space of VU m at slot t .
a_m	Abbreviation of $a_{m,t}$.	a'_m	Abbreviation of $a_{m,t+1}$.
a_m^i	Action of the i -th tuple in mini-batch.	$B_m(t)$	Buffer length of VU m at slot t .
\mathcal{R}	Replay buffer.	D	Diameter of BS's coverage.
$d_{m,i}(t)$	Bits of user m processed locally at slot t .	$d_{m,o}(t)$	Bits of user m offload at slot t .
$d_m(t)$	Distance between user m and BS's antennas along the x -axis.	$e(t)$	Error vector of adjacent slots channel vector.
$f_m(t)$	CPU frequency of user m at slot t .	F_{max}	The maximum allowed CPU frequency.
$h_m^s(t)$	Small-scale Rayleigh fading channel gain of VU m at slot t .	$h_m^p(t)$	The large-scale fading coefficient reflects the path-loss of VU m at slot t .
h_r	Reference power gain at distance 1m.	$\mathbf{H}(t)$	Channel matrix between BS and every VU at slot t .
H	Height of BS.	I	Size of mini-batch.
K_{max}	The maximum episode in training stage.	i	Index of tuples in the mini-batch.
$J(\mu_m)$	Objective function.	L_m	CPU cycles needed for VU m process one bit.
$L(\zeta^m)$	Loss function.	N_j	Total number of time slots.
$\mathbf{n}(t)$	Noise of signal received by BS.	N	Number of antenna.
$\mathbf{P}_{m,j}(t)$	Location of VU m at slot t .	\mathbf{P}_B	Location of BS.
$p_{m,o}(t)$	Offload power offered by VU m at slot t .	$p_{m,l}(t)$	Local process power offered by VU m at slot t .
$P_{max,o}$	Maximum offload power.	$P_{max,l}$	Maximum local execution power.
$Q^{\mu_{\theta^m}}(s_{m,t}, a_{m,t})$	Action-value function of VU m following policy μ_{θ^m} .	$Q^{\zeta^m}(s_{m,t}, a_{m,t})$	Action-value function approximated by critic-network.
$Q^{\zeta^{m'}}(s_{m,t}, a_{m,t})$	Action-value function of VU m approximated by target critic-network.	$r_{m,t}$	Reward of VU m slot t .
r_m^i	Reward of the i -th tuple in mini-batch.	r_m	Abbreviation of $r_{m,t}$.
\mathcal{R}	Replay buffer.	$s_{m,t}$	State space of VU m lot t .
s_m	Abbreviation of $s_{m,t}$.	s'_m	Abbreviation of $s_{m,t+1}$.
s_m^i	State of the i -th tuple in mini-batch.	$s_m^{i'}$	Next state of the i -th tuple in mini-batch.
\mathcal{T}_j	Set of time slots index.	v_j	Velocities of vehicles driven on lane j .
v_m	velocity of vehicular user m .	w_0	The width between the VU driven on the lane 1 and BS's antennas along y -axis.
w	Width of roads.	$w_{m,j}$	Width between VU m driven on lane j and antennas along the y -axis.
W	Bandwidth.	$\mathbf{y}(t)$	Signal received by BS.
y_m^i	Target value.	α_m^C	Learning rate of critic network.
α_m^A	Learning rate of actor network.	γ	Discounting factor of long-term reward.
$\gamma_m(t)$	SINR of VU m at slot t .	Δ_t	The exploration noise at slot t .
ζ^m	Parameter of critic network.	ζ^{m*}	Optimized parameter of critic network.
$\zeta^{m'}$	Parameter of target critic-network.	$\zeta^{m'*}$	Optimized parameter of target critic-network.
η	path-loss exponent.	θ^m	Parameter of actor network.
θ^{m*}	Optimized parameter of actor network.	$\theta^{m'}$	Parameter of target actor-network.
$\theta^{m'*}$	Optimized parameter of target actor-network.	θ_N	Decay-rate of Ornstein-Uhlenbeck noise for exploration.
κ_m	Effective switched capacitance of user m .	λ_m	Mean rate of tasks arrival for VU m .
μ_{θ^m}	Policy of VU m approximated by actor network.	μ_m^*	Optimal policy of VU m .
ρ_m	Normalized channel correlation coefficient of user m between adjacent slots.	σ	Variation of Ornstein-Uhlenbeck noise for exploration.
σ_R^2	Additive white Gaussian noise variance of the signal received by BS.	τ	Update parameter for target networks.
τ_0	Slot duration.	ω_1, ω_2	Weighted factors of reward.

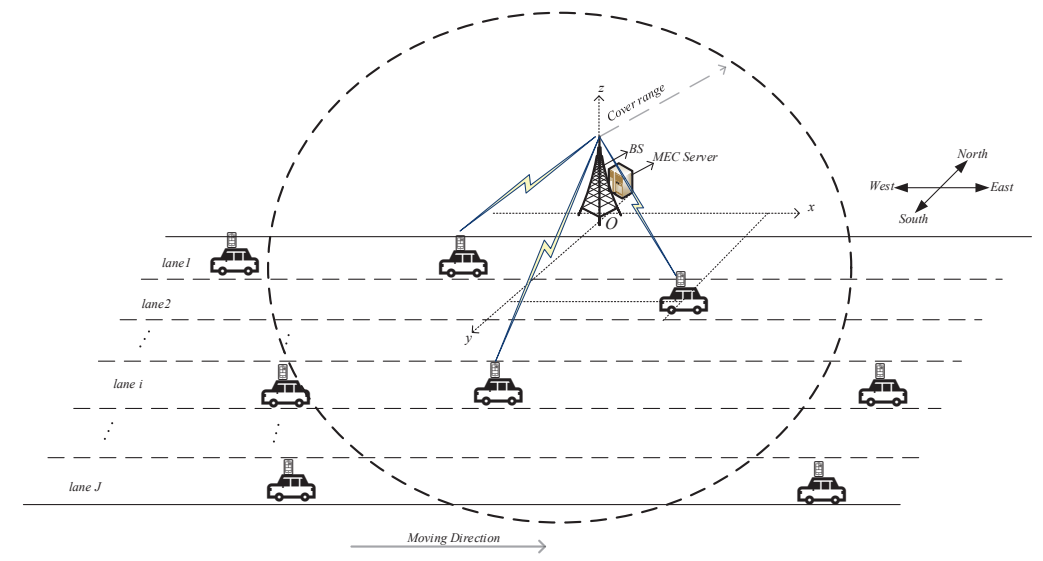


Fig. 1: System model.

offloading, each VU first transmits tasks to the BS, then the BS processes the tasks and adopts the zero-forcing (ZF) technique to detect the received signal and noise of each VU from the received signal of all VUs and further determines the signal-to-interference-plus-noise ratio (SINR) of each VU. Afterwards the BS sends back the computation results as well as the determined SINR to each VU at the next slot. Different from the traditional centralized DRL-based offloading scheme in VEC, in this paper each VU can distributively determine the power allocation based on its local information. Next, we will introduce the computation model, network model and mobility model to formulate the local information of VU m such as the buffer length, SINR and position, respectively. For simplicity, the notations adopted in this paper are listed as TABLE I.

A. Mobility model

Let $\mathbf{P}_{m,j}(t)$ be the position of VU m which moves on lane j at slot t . A space rectangular coordinate system shown in Fig. 1 is set to illustrate the positions of each VU and the BS, where the origin is the position of the BS, the direction of the x -axis is the moving direction of VUs, i.e., east, the direction of the y -axis is south, the direction of z -axis is set along the antennas of BS which is perpendicular to both x -axis and y -axis. Let $d_m(t)$ and $w_{m,j}$ be the distances between VU m and the antennas of BS along x -axis and y -axis at slot t , respectively. Thus $\mathbf{P}_m(t)$ is denoted as $(d_m(t), w_{m,j}, 0)$ in the space rectangular coordinate system, where $w_{m,j}$ depends on the lane index of VU m , i.e., j , and is calculated

as

$$w_{m,j} = (j - 1) \cdot w + w_0, \quad (1)$$

here w is the width of a lane and w_0 is the distance between lane 1 and the BS's antennas along y -axis.

Similar to [32], the position of VU m is approximately constant within each time slot due to the sufficiently small value of τ_0 . Since VU m moves on lane j with a constant velocity v_j , $d_m(t)$ is updated as

$$d_m(t) = d_m(t - 1) + v_j \tau_0, d_m(t) \in [-\frac{D}{2}, \frac{D}{2}], \quad (2)$$

where D is the coverage of the BS and $d_m(1) = -\frac{D}{2}$. VU m communicates with the BS once it enters the coverage of the BS and calculates $d_m(t)$ at each slot t according to Eq. (2). Therefore, $d_m(t)$ is a local observation of VU m at slot t to reflect the mobility of VU m .

B. Network model

The channel matrix at slot t can be expressed as $\mathbf{H}(t) = [\mathbf{h}_1(t), \dots, \mathbf{h}_m(t), \dots, \mathbf{h}_M(t)] \in \mathbb{C}^{N \times M}$, where $\mathbf{h}_m(t) \in \mathbb{C}^{N \times 1}$ is the channel vector between VU m and BS. In the MIMO-NOMA channel, the signal received by BS at slot t is the signal transmitted from all VUs, which can be expressed as

$$\mathbf{y}(t) = \sum_{m \in \mathcal{M}} \mathbf{h}_m(t) \sqrt{p_{m,o}(t)} s_m(t) + \mathbf{n}(t), \quad (3)$$

$$p_{m,o}(t) \in [0, P_{max,o}],$$

where $p_{m,o}(t)$ is the offloading power of VU m at t , $P_{max,o}$ is the maximum offloading power, $s_m(t)$ is the complex data symbol with unit variance, and $\mathbf{n}(t)$ is the vector of additive white Gaussian noise (AWGN) with variance σ_R^2 , (i.e., $\mathbf{n}(t) \sim \mathcal{CN}(\mathbf{0}, \sigma_R^2 \mathbf{I}_N)$, and \mathbf{I}_N is an $N \times N$ identity vector). Furthermore, $\mathbf{h}_m(t)$ is an integrated one of the stochastic small-scale fading channel gain $\mathbf{h}_m^s(t)$ and the large-scale fading coefficient $h_m^p(t)$ which reflects the path-loss of VU m [14], i.e.,

$$\mathbf{h}_m(t) = \mathbf{h}_m^s(t) \sqrt{h_m^p(t)}. \quad (4)$$

In Eq. (4), $h_m^p(t)$ characterizes the mobility of VU m and is calculated as

$$h_m^p(t) = \frac{h_r}{\|\mathbf{P}_{m,j}(t) - \mathbf{P}_B\|^\eta}, \quad (5)$$

where η is the path-loss exponent, h_r is the channel power gain at 1 meter distance, $\mathbf{P}_{m,j}(t) = (d_m(t), w_{m,j}, 0)$ is the position of VU m at slot t and \mathbf{P}_B is the position of antennas of BS. Note

that $w_{m,j}$ is calculated according to Eq. (1) and $d_m(t)$ is calculated according to Eq. (2). Let H be the height of antennas of BS, thus $\mathbf{P}_B = (0, 0, H)$.

In addition, the following autoregressive (AR) model is adopted to formulate the relationship between $\mathbf{h}_m^s(t)$ and $\mathbf{h}_m^s(t-1)$ [33], i.e.,

$$\mathbf{h}_m^s(t) = \rho_m \mathbf{h}_m^s(t-1) + \sqrt{1 - \rho_m^2} \mathbf{e}(t), \quad (6)$$

where ρ_m is the normalized channel correlation coefficient between the consecutive slots, $\mathbf{e}(t)$ is the error vector which obeys the complex Gaussian distribution and is correlated with $\mathbf{h}_m^s(t)$. According to Jake's fading spectrum, $\rho_m = J_0(2\pi f_d \tau_0)$, where f_d is the Doppler frequency and $J_0(\cdot)$ is the zeroth-order Bessel function of the first kind [34].

Then the BS adopts the pseudo inverse of $\mathbf{H}(t)$, which is denoted as $\mathbf{H}^\dagger(t)$, as the ZF detector to detect the received signal of VU m from $\mathbf{y}(t)$. According to [33], $\mathbf{H}^\dagger(t)$ is calculated as

$$\mathbf{H}^\dagger(t) = (\mathbf{H}^H(t)\mathbf{H}(t))^{-1} \mathbf{H}^H(t), \quad (7)$$

where $\mathbf{H}^H(t)$ is the conjugate transpose of $\mathbf{H}(t)$.

Specifically, letting $\mathbf{g}_m^H(t)$ be the m -th row of $\mathbf{H}^\dagger(t)$, by multiplying $\mathbf{y}(t)$ with $\mathbf{g}_m^H(t)$, we can obtain the following equation according Eq. (3):

$$\mathbf{g}_m^H(t)\mathbf{y}(t) = \mathbf{g}_m^H(t) \sum_{m \in \mathcal{M}} \mathbf{h}_m(t) \sqrt{p_{m,o}(t)} s_m(t) + \mathbf{g}_m^H(t)\mathbf{n}(t). \quad (8)$$

Since $\mathbf{g}_m^H(t)$ is the m -th row of $\mathbf{H}^\dagger(t)$, according to Eq. (7), we have

$$\mathbf{g}_m^H(t)\mathbf{h}_i(t) = \delta_{m,i}(t) = \begin{cases} 1, & i = m \\ 0, & i \neq m \end{cases} \quad (9)$$

Substituting Eq. (9) into Eq. (8), we have

$$\mathbf{g}_m^H(t)\mathbf{y}(t) = \sqrt{p_{m,o}(t)} s_m(t) + \mathbf{g}_m^H(t)\mathbf{n}(t), \quad (10)$$

where $\sqrt{p_{m,o}(t)} s_m(t)$ is the signal received by BS from VU m , $\sqrt{p_{m,o}(t)}$ is the power of the received signal, and $\mathbf{g}_m^H(t)\mathbf{n}(t)$ is the noise of VU m received by BS. Since the power of $\mathbf{n}(t)$ is σ_R^2 , the noise power is calculated as $\|\mathbf{g}_m^H(t)\|^2 \sigma_R^2$. Thus, the SINR of VU m can be calculated as

$$\gamma_m(t) = \frac{p_{m,o}(t)}{\|\mathbf{g}_m^H(t)\|^2 \sigma_R^2}. \quad (11)$$

The BS can detect the SINR of VU m at slot t , i.e., $\gamma_m(t)$, according to Eqs. (3)-(11) and transmit $\gamma_m(t)$ to VU m at next slot. In this case, VU m receives $\gamma_m(t-1)$ at slot t and thus $\gamma_m(t-1)$ is also a local observation of VU m at slot t to reflect the channel variation.

C. Computation model

For VU m , the buffer length of VU m at slot t is denoted as $B_m(t)$ and the relationship between $B_m(t)$ and $B_m(t-1)$ is expressed as

$$B_m(t) = [B_m(t-1) - (d_{m,o}(t-1) + d_{m,l}(t-1))]^+ + a_m(t-1), \quad (12)$$

where $[\cdot]^+ = \max(0, \cdot)$, $a_m(t-1)$ is the amount of the tasks arriving at the buffer queue of VU m at slot $t-1$, $d_{m,l}(t-1)$ and $d_{m,o}(t-1)$ are the amount of the tasks processed by local execution and offloaded to the BS at slot $t-1$, respectively. Therefore the amount of tasks departing from the buffer at slot $t-1$ becomes $d_{m,l}(t-1) + d_{m,o}(t-1)$, which should not exceed $B_m(t-1)$. We will also explain how $d_{m,l}(t-1)$ and $d_{m,o}(t-1)$ are determined as follows.

1) *Local execution*: Let L_m be the computation intensity of tasks (i.e., the number of CPU cycles required to processed one bit data), $f_m(t-1)$ be the CPU frequency of VU m at slot $t-1$. The task size that can be processed by local execution at slot $t-1$ is calculated as

$$d_{m,l}(t-1) = \tau_0 f_m(t-1) / L_m. \quad (13)$$

Letting $p_{m,l}(t-1)$ be the local execution power at slot $t-1$, $f_m(t-1)$ is calculated as

$$f_m(t-1) = \sqrt[3]{p_{m,l}(t-1) / \kappa}, \quad (14)$$

$$p_{m,l} \in [0, P_{max,l}], f_m(t-1) \in [0, F_{max}],$$

where κ is the effective switched capacitance, $P_{max,l}$ is the maximum local execution power, F_{max} is the maximum CPU frequency. According to Eq. (14), F_{max} can be calculated as $F_{max} = \sqrt[3]{P_{max,l} / \kappa}$.

2) *Offloading*: In the offloading mode, the computation resources of VEC server are sufficient, thus the latency that the VEC server processes the tasks is negligible. In addition, the size of computation result is usually very small, thus the feedback delay can also be ignored. Therefore, the delay of task transmission is the duration of a slot τ_0 . In this case, the amount of tasks processed by offloading at slot $t-1$ can be calculated according to Shannon theory, i.e.,

$$d_{m,o}(t-1) = \tau_0 W \log_2(1 + \gamma_m(t-1)), \quad (15)$$

where W is the bandwidth and $\gamma_m(t-1)$ is the SINR of VU m at slot $t-1$.

Since VU m receives its SINR information $\gamma_m(t-1)$ from the BS at slot t , it allocates $p_{m,l}(t-1)$ and observes $a_m(t-1)$ at slot $t-1$. In this case, VU m can calculate $B_m(t)$ at slot t according to Eqs. (12)-(15) given $L_m, \kappa, P_{max}, \tau_0$ and W and thus $B_m(t)$ is another local observation of VU m at slot t to reflect the stochastic task arrival and the uncertain channel condition.

IV. PROBLEM FORMULATION

In the system, statistics task arrival and uncertain channel condition are all unknown to each VU, thus we adopt DRL framework which includes state, action, policy and reward to formulate the power allocation problem in the VEC [12]. Specifically, for each VU at each slot t , VU observes the current local state s_t and makes action a_t based on s_t according to policy μ , i.e., the function that generates the action based on the state at each slot. Then VU receives a reward r_t and observes the state at the next slot s_{t+1} , which is transited from the current state s_t . Next the state s_t , action a_t and reward r_t of VU at slot t will be defined, respectively.

A. State

Different from the traditional centralized DRL-based offloading scheme in VEC, each VU observes its local state to determine the power allocation in this paper. Since the power consumption and delay are impacted by the stochastic task arrival and uncertain channel condition caused by the MIMO-NOMA channel interference and mobility of VUs, the local state should be selected to reflect the stochastic task arrival and uncertain channel condition as well as the mobility of the VU.

In the system model, the distance between VU m , and the antennas of the BS along x -axis at slot t , i.e., $d_m(t)$, determines the position of VU m at slot t , which reflects the mobility of VU m . In addition, according to Eq. (11), the SINR of VU m at slot t , i.e., $\gamma_m(t-1)$, depends on $\mathbf{g}_m^H(t-1)$ that is related with the channel vector $\mathbf{h}_m(t-1)$, and thus $\gamma_m(t-1)$ can reflect the uncertain channel condition at slot t . Moreover, according to Eqs. (12)-(15), the buffer length of VU m at slot t , i.e., $B_m(t)$, is a function of $a_m(t-1)$ and $\gamma_m(t-1)$, where $a_m(t-1)$ reflects the stochastic task arrival and $\gamma_m(t-1)$ reflects the uncertain channel condition. Therefore, $B_m(t)$ reflects both stochastic task arrival and uncertain channel condition. As shown in the system model, $B_m(t)$, $\gamma_m(t-1)$ and $d_m(t)$ are all the local observations of VU m at slot t , therefore the state of VU m at slot t can be defined as

$$s_{m,t} = [B_m(t), \gamma_m(t-1), d_m(t)]. \quad (16)$$

where $\gamma_m(t-1)$ depends on $\mathbf{h}_m(t-1)$ and $B_m(t)$ depends on $\gamma_m(t-1)$ and $a_m(t-1)$. Since $a_m(t-1)$ and $\mathbf{h}_m(t-1)$ are random values within continuous space, thus the state space of VU is continuous.

B. Action

Each VU m allocates the local execution power and offloading power based on the local observed state $s_{m,t}$, thus the local execution and offloading power are defined as the action of VU m at slot t , i.e.,

$$a_{m,t} = [p_{m,o}(t), p_{m,l}(t)]. \quad (17)$$

Note that similar to [35], we consider the fine-grained computation applications, thus VU m allocates the local execution and offloading power within continuous spaces in $[0, P_{m,l}]$ and $[0, P_{m,o}]$ to process the tasks, respectively. In this case the action space of VU m is continuous.

C. Reward function

In this paper, VU m aims to improve the network performance in terms of the power consumption and delay. As described in the computation model, the latency of task processing at the VEC server is negligible and the feedback delay during the offloading is also ignored at each slot. In this case the delay of task transmission is a constant, i.e., the duration of a slot. Thus the delay consumed by VU m is impacted by the buffer delay that is proportional to the average buffer length according to the Little's Theorem [36]. Therefore, the reward function of VU m at slot t is defined as

$$r_{m,t} = -[\omega_1 (p_{m,o}(t) + p_{m,l}(t)) + \omega_2 B_m(t)], \quad (18)$$

where ω_1 and ω_2 are the nonnegative weighted factors.

The expected long-term discounted reward of VU m is calculated as

$$J(\mu_m) := \mathbb{E}_{\mu_m} \left[\sum_{t=1}^{N_j} \gamma^{t-1} r_{m,t} \right], \quad (19)$$

where $\gamma \in [0, 1]$ is the discounting factor and N_j is the upper limit of slot index when VU m moves on lane j . In this paper, we aim to find the optimal policy μ_m^* to maximize the expected long-term discounted reward of VU m .

V. SOLUTION

In this section, we first describe the training stage to obtain the optimal policy, then introduce the testing stage to test the performance under the optimal policy.

A. Training stage

Since the state and action spaces are continuous and the DDPG algorithm is suitable to solve the DRL-based problem under the continuous state and action space. Therefore, we utilize the DDPG algorithm to obtain the optimal policy in the training stage.

Algorithm 1: Training Stage for the DDPG based Framework

Input: $\gamma, \tau, \theta^m, \zeta^m$
Output: optimized θ^{m*}, ζ^{m*}

- 1 Randomly initialize the θ^m, ζ^m ;
- 2 Initialize target networks by $\zeta^{m'} \leftarrow \zeta^m, \theta^{m'} \leftarrow \theta^m$;
- 3 Initialize replay experience buffer \mathcal{R} ;
- 4 **for** *episode* from 1 to K_{max} **do**
- 5 Reset simulation parameters for the VEC system model;
- 6 Receive initial observation state s_1 ;
- 7 **for** *time slot* t from 1 to N_j **do**
- 8 Generate the power for local process and computation offloading according to the current policy and exploration noise $a_m = \mu_{\theta^m}(s_m|\theta^m) + \Delta_t$;
- 9 Execute action a_m , observe reward r_m and new state s'_m from the system model;
- 10 Store transition (s_m, a_m, r_m, s'_m) in \mathcal{R} ;
- 11 **if** *number of tuples in \mathcal{R} is larger than I* **then**
- 12 Randomly sample a mini-batch of I transitions tuples from \mathcal{R} ;
- 13 Update the critic network by minimizing the loss function according to Eq. (23);
- 14 Update the actor network according to Eq. (24);
- 15 Update target networks according to Eqs. (25) and (26).

The DDPG algorithm is based on actor-critic architecture. The actor is applied for policy improvement, and the critic is applied for policy evaluation. The DDPG algorithm adopts deep neural network (DNN) on actor and critic to efficiently approximate and evaluate the policy, respectively, thus forming the corresponding actor network and critic network. The actor network is used to approximate the policy μ_m , where the approximated policy is denoted as μ_{θ^m} , the output of the actor network is the action based on the policy μ_{θ^m} and observed state. In the DDPG algorithm, the optimal policy is obtained through iterative policy improvement and evaluation. Moreover, DDPG algorithm adopts the target networks including target actor network and target critic network to guarantee the stability of the algorithm. The architecture of target actor-network and target critic-network are the same with the actor network and critic network, respectively. The pseudocode of the proposed algorithm is described in Algorithm 1. Let θ^m and ζ^m be the parameters of the actor network and critic network, respectively, and $\theta^{m'}$ and $\zeta^{m'}$ be the parameters of the target actor network and target critic network, respectively, Δ_t be the noise for action exploration at slot t . For ease of understanding, we further introduce the DDPG algorithm in detail

as follows.

Firstly, θ^m and ζ^m are initialized randomly, while $\theta^{m'}$ and $\zeta^{m'}$ are initialized as θ^m and ζ^m , respectively. A replay buffer \mathcal{R} with sufficient space is constructed to cache transition at each slot (lines 1-3).

Then the algorithm is executed for K_{max} episodes. In the first episode, the position of VU m ($d_m(1), w_{m,j}, 0$) is reset as the position that it enters the coverage area of the BS, i.e., $d_m(1)$ is set as $-\frac{D}{2}$, and $B_m(1)$ is initialized as half of the buffer size. Then $\mathbf{h}_m^s(0)$ is initialized randomly, and $\mathbf{g}_m(0)$ is calculated according to Eq. (7) based on $\mathbf{h}_m^s(0)$, given the $\mathbf{g}_m(0)$ the initial SINR $\gamma_m(0)$ is calculated according to Eq. (11). Thus, VU m can observe the state at slot 1, i.e., $s_{m,1} = [B_m(1), \gamma_m(0), d_m(1)]$ (line 4-6).

Afterwards, the algorithm is executed iteratively from slot 1 to slot N_j . Given the input $s_{m,1}$ the output of the actor network is $\mu_{\theta^m}(s_{m,1}|\theta^m)$. As a noise Δ_1 is generated randomly and VU m sets the action $a_{m,1}$ as $\mu_{\theta^m}(s_{m,1}|\theta^m) + \Delta_1$, thus the offloading power $p_{m,o}(1)$ and local execution power $p_{m,l}(1)$ are determined. Then, VU m allocates offloading power and local execution power to process the task, while achieving the reward $r_{m,1}$ according to Eq. (13). Then, BS adopts the ZF technology to determine the SINR $\gamma_m(1)$. Specifically, BS collects the channel vector of each vehicle, calculates $\mathbf{g}_m(1)$ according to Eq. (7), and then determines the initial SINR $\gamma_m(1)$ according to Eq. (11) under the obtained $\mathbf{g}_m(1)$. Afterwards VU m observes the next state $s_{m,2} = [B_m(2), \gamma_m(1), d_m(2)]$. Specifically, VU m calculates $B_m(2)$ according to Eq. (8), where $d_{m,l}(1)$ is calculated based on Eqs. (13)-(14) under $p_{m,l}(1)$ and $d_{m,o}(1)$ is calculated according to Eq. (15) under $p_{m,o}(1)$. In addition, VU m receives its SINR $\gamma_m(1)$ from BS. Moreover, VU m calculates $d_m(2)$ according to Eq. (2) given the position $d_m(1)$. Then the tuple $(s_{m,1}, a_{m,1}, r_{m,1}, s_{m,2})$ is stored in the replay buffer. When the number of tuples stored in the replay buffer is less than I , VU m inputs the next state into the actor network and begins the next iteration (lines 7-10).

When the number of the stored tuples is larger than I , the parameters of actor network, critic network and target networks, i.e., θ^m , ζ^m , $\theta^{m'}$ and $\zeta^{m'}$, are updated iteratively to maximize $J(\mu_{\theta^m})$. The parameters of actor-network θ^m is updated with the policy gradient, i.e., updating θ^m toward the direction of the gradient of $J(\mu_{\theta^m})$, which is denoted as $\nabla_{\theta^m} J(\mu_{\theta^m})$. Let $Q^{\mu_{\theta^m}}(s_{m,t}, a_{m,t})$ be the action-value function of VU m following policy μ_{θ^m} under $s_{m,t}$ and $a_{m,t}$, which stands for the expected discounted long-term reward of VU m from slot t , i.e.,

$$Q^{\mu_{\theta^m}}(s_{m,t}, a_{m,t}) := \mathbb{E}_{\mu_{\theta^m}} \left[\sum_{k=t}^{N_j} \gamma^{k-t} r_{m,k} \right]. \quad (20)$$

In [37], Silver *et al.* proved that solving $\nabla_{\theta^m} J(\mu_{\theta^m})$ can be substituted by solving the gradient of

$Q^{\mu_{\theta^m}}(s_{m,t}, a_{m,t})$, which is denoted as $\nabla_{\theta^m} Q^{\mu_{\theta^m}}(s_{m,t}, a_{m,t})$. However, $Q^{\mu_{\theta^m}}(s_{m,t}, a_{m,t})$ in Eq. (17) can not be calculated by Bellman equation due to the continuous action space [38]. To address this issue, the critic network adopts DNN parameterized by ζ^m to approximate the action-value function $Q^{\mu_{\theta^m}}(s_{m,t}, a_{m,t})$, the action-value function approximated by critic-network is denoted as $Q^{\zeta^m}(s_{m,t}, a_{m,t})$.

The iteration in slot t ($t = 1, 2, \dots, N_j$) to update θ^m , ζ^m , $\theta^{m'}$ and $\zeta^{m'}$ is described as follows when the number of the stored tuples is larger than I . For simplicity, $r_{m,t}$, $s_{m,t}$, $a_{m,t}$, $s_{m,t+1}$ and $a_{m,t+1}$ are expressed as r_m , s_m , a_m , s'_m and a'_m , respectively. VU m first uniformly samples I tuples from replay buffer to form a mini-batch. Let $(s_m^i, a_m^i, r_m^i, s'^i_m, a'^i_m)$ ($i = 1, 2, \dots, I$) be the i -th tuple in the mini-batch. Then VU m inputs each tuple into the target actor-network, target critic network and critic network. For tuple i , VU m first inputs s'^i_m into the target actor-network and outputs the action $a'^i_m = \mu_{\theta^{m'}}(s'^i_m | \theta^{m'})$, then VU m inputs s^i_m and a'^i_m into the target critic-network and outputs the action-value function $Q^{\zeta^{m'}}(s^i_m, a'^i_m)$. After that VU m calculates the target value as

$$y_m^i = r_m^i + \gamma Q^{\zeta^{m'}}(s^i_m, a'^i_m) |_{a'^i_m = \mu_{\theta^{m'}}(s'^i_m | \theta^{m'})}. \quad (21)$$

Then, given the s^i_m and a^i_m , the critic network achieves outputs such as the action-value function $Q^{\zeta^m}(s^i_m, a^i_m)$, and then calculates the loss of tuple i as

$$L_i = \left[y_m^i - Q^{\zeta^m}(s^i_m, a^i_m) \right]^2. \quad (22)$$

After VU m inputs all tuples into the target actor-network, target critic network and critic network, VU m calculates the loss function as

$$L(\zeta^m) = \frac{1}{I} \sum_{i=1}^I L_i, \quad (23)$$

then Adam optimization with learning rate α_m^C is adopted to update the parameters of the critic-network ζ^m towards the gradient $\nabla_{\zeta^m} L(\zeta^m)$ [39]. (lines 11-13)

Similarly, VU m adopts Adam optimization [39] with learning rate α_m^A to update the parameters of the actor-network θ^m towards the gradient $\nabla_{\theta^m} J(\mu_{\theta^m})$ [39], where $\nabla_{\theta^m} J(\mu_{\theta^m})$ is calculated by the action-value function which is approximated by critic-network, i.e., (line 14)

$$\begin{aligned} & \nabla_{\theta^m} J(\mu_{\theta^m}) \\ & \approx \frac{1}{I} \sum_{i=1}^I \nabla_{\theta^m} Q^{\zeta^m}(s^i_m, a^i_m) |_{a^i_m = \mu_{\theta^m}(s^i_m | \theta^m)} \\ & = \frac{1}{I} \sum_{i=1}^I \nabla_{a^i_m} Q^{\zeta^m}(s^i_m, a^i_m) |_{a^i_m = \mu_{\theta^m}(s^i_m | \theta^m)} \cdot \nabla_{\theta^m} \mu_{\theta^m}(s^i_m | \theta^m). \end{aligned} \quad (24)$$

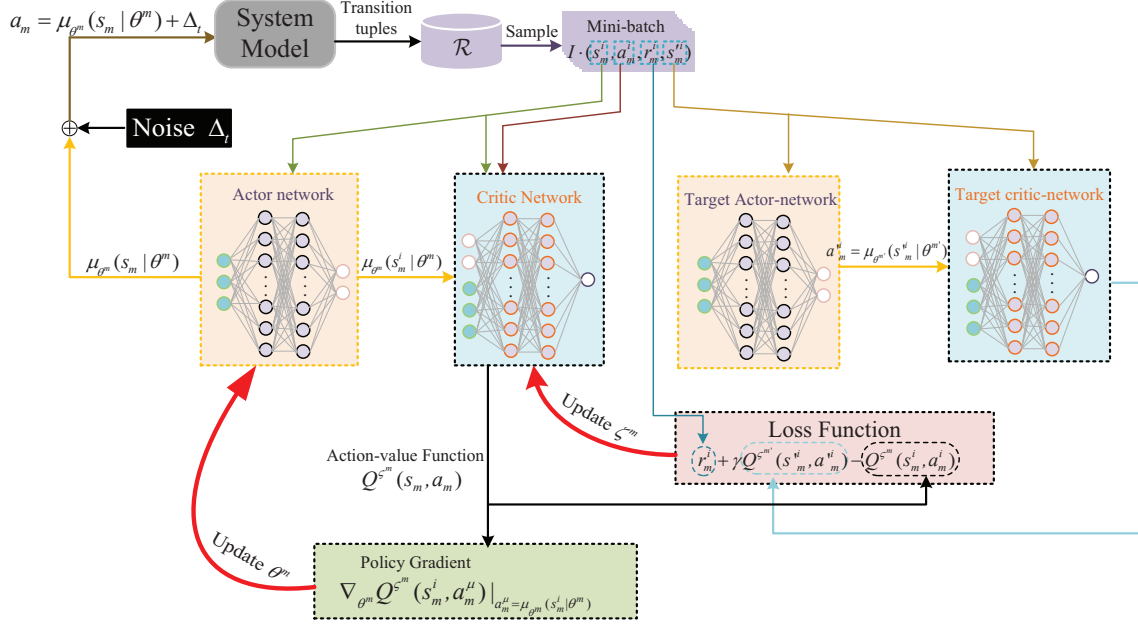


Fig. 2: Flow Diagram of DDPG

At the end of slot t , VU m updates the parameters of the target actor-network and target critic-network as

$$\zeta^{m'} \leftarrow \tau \zeta^m + (1 - \tau) \zeta^{m'}, \quad (25)$$

$$\theta^{m'} \leftarrow \tau \theta^m + (1 - \tau) \theta^{m'}, \quad (26)$$

where τ is a constant satisfying $\tau \ll 1$ (line 15).

Finally, VU m input s'_m into the actor network and begins the iteration in next slot. The episode is finished when the number of iterations reaches N_j . Then VU m will initialize $B_m(1)$, $\gamma_m(0)$, $d_m(1)$ and start the next episode. The algorithm will finally terminate when number of episode reaches K_{max} and provides the optimized parameters of actor network, critic network and target actor-network, target critic-network, denoted as θ^{m*} , ζ^{m*} , $\theta^{m'*}$ and $\zeta^{m'*}$, respectively, which means that the training stage is finished and the optimal policy μ_m^* , i.e., the optimal power allocation scheme, is the approximated policy of the actor network under the optimized parameters θ^{m*} . The flow diagram of the DDPG algorithm is shown in Fig. 2.

B. Testing stage

The testing stage omits the critic network, target actor-network and target critic-network in the training stage and employs the optimal policy with optimized parameter θ^{m*} to test the performance. The pseudocode of the testing stage is shown in Algorithm 2.

Algorithm 2: Testing Stage for the DDPG based Framework

```

1 for episode from 1 to  $K'_{max}$  do
2   Reset simulation parameters for the VEC system model;
3   Receive initial observation state  $s_1$ ;
4   for time slot  $t$  from 1 to  $N_j$  do
5     Generate the power for local process and computation offloading according to the optimal
       policy  $a_m = \mu_{\theta^m}(s_m|\theta^{m*})$ ;
6     Execute action  $a_m$ , observe reward  $r_m$  and new state  $s'_m$  from the system model.

```

VI. SIMULATION RESULTS AND ANALYSIS

In this section, we conduct simulation experiments to verify the effectiveness of the optimal power allocation scheme, i.e., the optimal policy, in the training and testing stage, respectively. The simulation tool is Python 3.6. The scenario is described in the system model. In the simulation experiments, both actor network and critic network are the four-layer fully connected DNN with two hidden layers which are equipped with 400 and 300 neurons, respectively. The noise Δ_t for exploration follows the Ornstein-Uhlenbeck (OU) process [40] with the decay-rate θ_N and variation σ . The size of experience replay buffer is $|\mathcal{R}|$. The task arrivals at each slot follow Poisson distribution with mean task arrival rate λ_m . The maximum local process power $P_{m,l}$ is calculated according to Eq. (14) given the maximum allowable CPU frequency F_{max} . The small scale fading of VU m is initialized as $\mathbf{h}_m^s(0) \sim \mathcal{CN}(\mathbf{0}, \mathbf{I}_N)$. The target

TABLE II: Values of the parameters in the experiments.

Parameters of System Model							
Parameter	Value	Parameter	Value	Parameter	Value	Parameter	Value
σ_R^2	10^{-9}W	h_r	-30dB	ρ	0.95	W	1Mhz
τ_0	20ms	κ	10^{-28}	v_1	20m/s	v_2	25m/s
v_3	30m/s	w	10m	L_m	500cycles/bit	λ_m	3Mbps
H	10m	N	4	D	500m	$P_{max,l}$	1W
$P_{max,o}$	1W	F_{max}	2.15GHz	J	3	w_0	10m
Parameters of DDPG							
Parameter	Value	Parameter	Value	Parameter	Value	Parameter	Value
α_m^C	0.001	α_m^A	0.0001	ω_1	0.9	ω_2	0.1
γ	0.99	τ	0.001	K_{max}	2000	σ	0.02
θ_N	0.15	I	64	K'_{max}	10	$ \mathcal{R} $	2.5×10^5

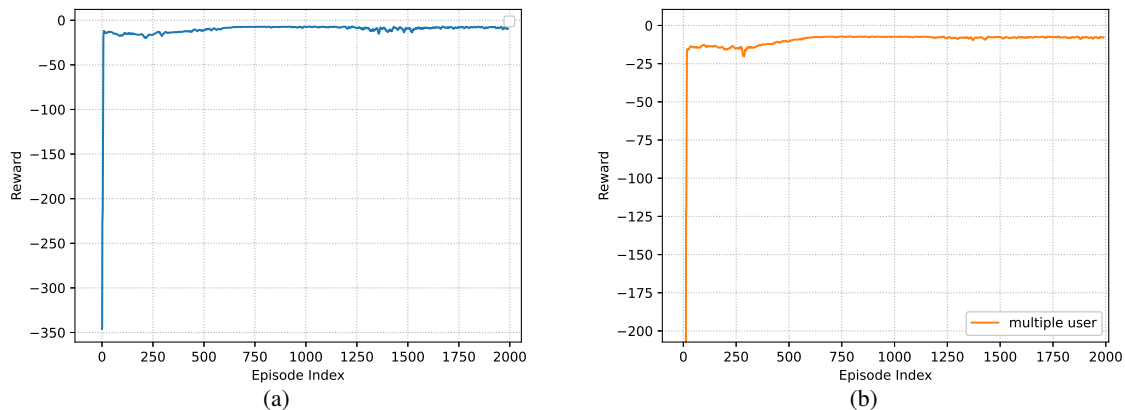


Fig. 3: Learning curve. (a) single-user scenario; (b) multi-user scenario.

VU, i.e., VU m , moves on lane 2 with velocity v_2 . The remaining parameters and algorithm parameters are shown in TABLE II.

A. Training Stage

Fig. 3-(a) shows the learning curve of training process in the single-user scenario, which reflects the average reward in each slot under different episodes. It can be seen that the average reward rises rapidly from episode 0 to episode 10, then the uptrend of the curve slows down from episode 10 to 600, which reflects that VU m is learning the policy efficiently toward the optimal reward. Then the reward turns to be stable from episode 600 to 1200, which means that the optimal policy has been learned. After that, there is a little jitter from episode 1200 to 1570. It is because the policy is adjusted slightly due to the exploration noise to prevent the policy from converging to local optimal value. Then, the curve turns to be stable again after episode 1500, which means the optimal policy has been learned again after the affection of the exploration noise.

Fig. 3-(b) shows the learning curve of the training process in multi-user scenario where three other VUs on each of three lanes drive into the coverage of BS at slot 500. It is seen that the trend of the curve is similar to that in the single-user scenario, which means that the proposed scheme is suitable for different dynamic scenarios.

B. Testing Stage

In the testing stage, VU m adopts learned policy in the testing stage to test the performance. Figs. 4-6 compare the testing performance including the power consumption, buffer length and reward at each slot under the optimal policy with that under greedy local execution first (GD-Local) and greedy offload

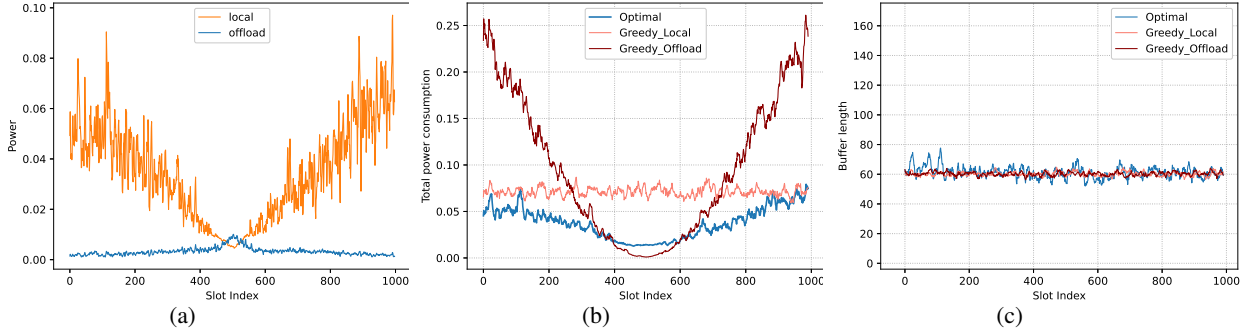


Fig. 4: Single-user scenario. (a) Power allocation; (b) Total power consumption; (c) Buffer length.

first (GD-Offload) policy, where the performance at each slot is obtained through averaging the results obtained in K'_{max} episodes. GD-Local policy and GD-Offload policy are introduced as follow.

- GD-Local policy: VU m firstly adopts the maximum local execution power to process tasks at each slot through local execution, while the remaining tasks are processed through offloading.
- GD-Offload policy: VU m firstly adopts the maximum offloading power to process tasks through offloading at each slot, while the remaining tasks are processed through local execution.

Fig. 4-(a), (b) and (c) show the testing performance in single-user scenario. Fig. 4-(a) compares the local execution power with the offloading power under the optimal policy. It is seen that from slot 0 to 500, the local execution power decreases obviously and offloading power increases slowly. After that, the local execution power increases obviously and offloading power decreases slowly. It is because that VU m is getting close to the BS from slot 0 to 500 and then getting far away from the BS after slot 500. According to Eq. (4), the channel condition is impacted by path-loss. When VU m is getting close to the BS, the path-loss is decreasing, thus leading to the better channel condition. Therefore, VU m will consume more offloading power and less local execution power to process more tasks when it gets close to the BS. On the contrary, VU m will consume less offloading power and more local execution power to process more tasks when it gets far away from the BS. Fig. 4-(b) shows the total power consumption which is the summation of the local execution and offloading power at each slot under the optimal policy, GD-Local and GD-Offload. It can be seen that similar to the local execution power under the optimal policy in Fig. 4-(a), the total power under the optimal policy and GD-Offload decreases from slot 0 to 500, and increases from slot 500 to 1000. This is because that the total power of the optimal policy is composed of both the local execution power and offloading power at each slot in Fig. 4-(a), where the local execution power overweighs offloading power. For the GD-Offload policy, the offloading power always keeps the maximum value, thus VU m will process more tasks through offloading when it gets

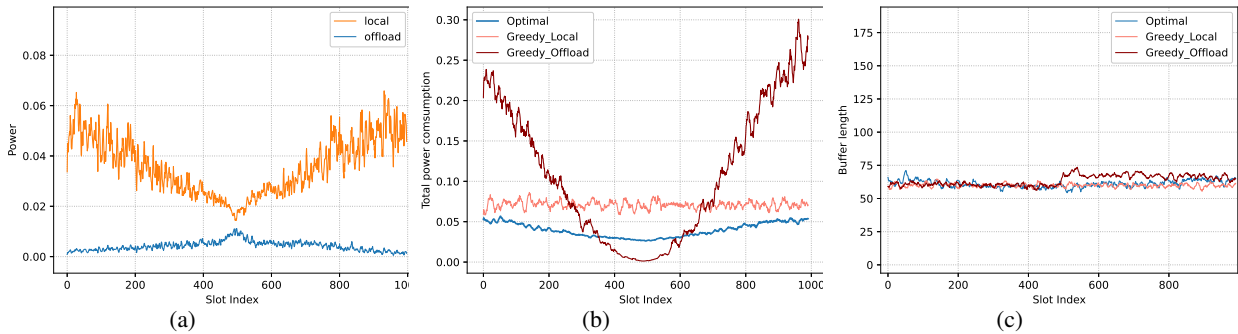


Fig. 5: Multi-user scenario. (a) Power allocation; (b) Total power consumption; (c) Buffer length.

close to the BS, which results in less local execution power consumption in the GD-Offload policy. In contrast, it consumes more local execution power when the VU gets far away from the BS. Moreover, it can be seen that the total power almost does not change at each slot in the GD-Local policy. This is because that the local execution power always keeps the maximum power, while the offloading power is much smaller than the local execution power, which can be ignored in the total power under the GD-Local policy. Fig. 4-(c) shows the buffer length under the optimal policy, GD-Local and GD-Offload, respectively. It is seen that the buffer length of the each policy fluctuates around the mean of tasks arrival, which is calculated as $\mathbb{E}[a(t)] = \tau_0 \lambda_m = 60 \text{ kbit}$, in each slot. It is because according to Eq. (12), almost all tasks arrive at previous time slot will be processed at the next time slot, which means that there is almost no buffer accumulation under the three policies.

Figs. 5-(a), (b) and (c) show the testing performance in the multi-user scenario. Fig. 5-(a) compares the local execution power with offloading power under the optimal policy. It is seen that different from the curves in Fig. 4-(a), the local execution power increases sharply from slot 500 to 600. This is because that three other vehicles drive into the BS's coverage area at slot 500, which imposes interference on VU m and incurs the deteriorated channel condition. In this case, VU m consumes more local execution power and less offloading power to process more tasks. Fig. 5-(b) shows the total power consumption under three policies. Different from Fig. 4-(b), VU m consumes more total power after slot 500 under the optimal policy. This is because that the channel is deteriorated due to the interference among VUs, thus VU m consumes more total power in the optimal policy. Fig. 5-(c) shows the buffer length at each slot under three policies. Different from Fig. 4-(b), the buffer length of GD-Offload is increased at slot 500. This is because that more task cached in the buffer owing to the deteriorated channel condition. Moreover, the buffer length of the optimal policy also fluctuates around the mean of tasks arrival, which means that VU m can process the tasks in time without increasing the buffer length in the multi-user

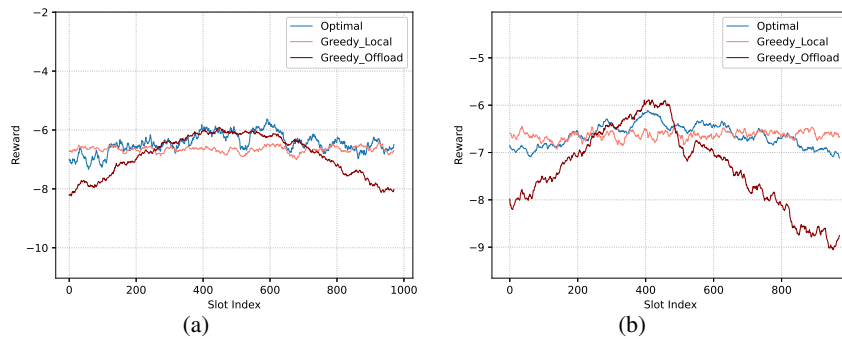


Fig. 6: Reward (a) Single-user scenario; (b) Multi-user scenario.

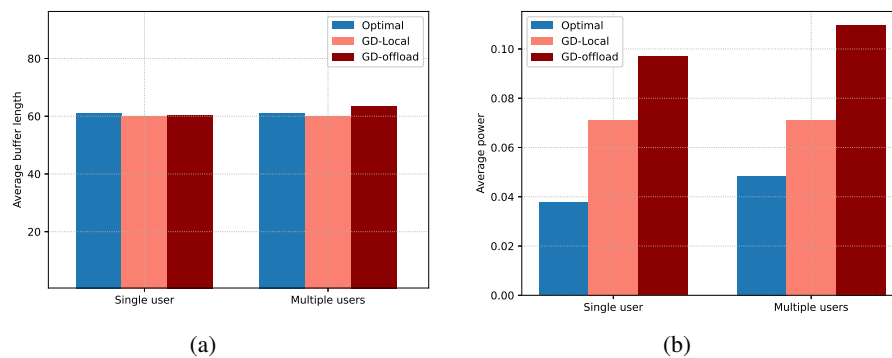


Fig. 7: Average buffer length and power consumption (a) Average buffer length; (b) Average power consumption.

scenario.

Figs. 6-(a) and (b) illustrate the reward of VU m in different scenarios. Fig. 6-(a) shows the reward at each slot under three policies in the single-user scenario, which is calculated according to Eq. (18). It is seen that the reward of the optimal policy is almost always larger than that of other two policies. This is attribute to the fact that the optimal policy considers the channel condition to adjust the power allocation adaptively to maximize the long-term reward. Fig. 6-(b) compares the rewards of the three policies in multi-user scenario. Similarly, the reward of the optimal policy is almost always larger than the that of other two policies owing to the adaptive power allocation.

Fig. 7-(a) shows the average buffer length under three policies in the single-user and multi-user scenarios, where the average buffer length in single-user and multi-user scenario are obtained by averaging the results at all slots in Figs. 4-(c) and 5-(c), respectively. It can be seen that the average buffer lengths under the policies for both multi-user and single-user scenarios which are nearly equal to the mean of tasks arrival rate in each slot and do not change significantly. Fig. 7-(b) shows the average power consumption

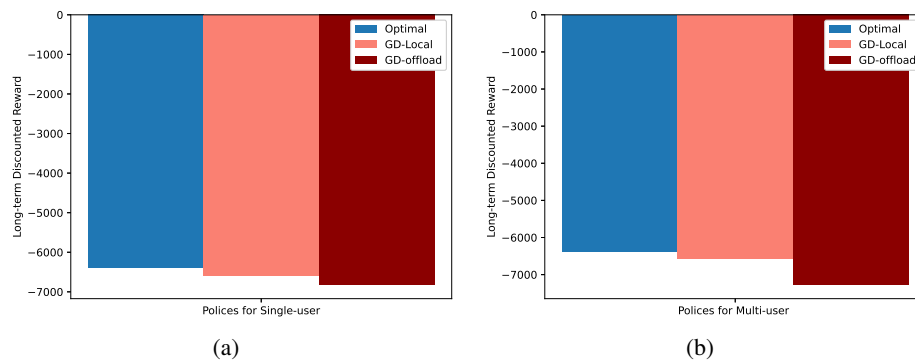


Fig. 8: Long-term discounted reward (a) Single-user scenario; (b) Multi-user scenario.

under three policies in the single-user and multi-user scenario, where the average power consumption in the single-user and multi-user scenario are obtained by averaging the results at all slots in Figs. 4-(b) and 5-(b), respectively. It is seen that compared with GD-Local, the average power consumption of the optimal policy is reduced by 47% and 27% in single-user and multi-user scenario, respectively. Compared with GD-Offload, the average power consumption of the optimal policy is reduced by 61% and 53% in single-user and multi-user scenario, respectively. Moreover, due to the worse channel in the multi-user scenario, the power consumption of the optimal policy and GD-offload in multi-user scenario is higher than that in the single-user scenario. However, the average power consumption of GD-Local almost keeps the same in the two scenarios. This is because the local execution power always keeps the maximum value, while the offloading power is much smaller than the local execution power, and thus can be ignored in the total power under the GD-Local policy.

Figs. 8-(a) and (b) compare the long-term discounted reward under the three policies in both the single-user scenario and multi-user scenario, respectively. As one can see, for both single-user scenario and multi-user scenario the optimal policy always has a higher the long-term discounted reward than other policies. This is because the optimal policy can adaptively adjust power allocation to maximize the long-term discounted reward.

Figs. 9-(a), (b) and (c) illustrate the long-term discounted reward, power consumption and buffer length of the three policies under different task arrivals in the single-user scenario, respectively. It can be seen that the long-term discounted rewards of the three policies decrease as the task arrival rate increases. As seen, increasing task arrival will lead to more power consumption and longer buffer length, thus degrading the reward according to Eq. (18). It also can be seen that the optimal policy outperforms GD-Local and GD-Offload policies in terms of power consumption and long-term discounted reward, but it

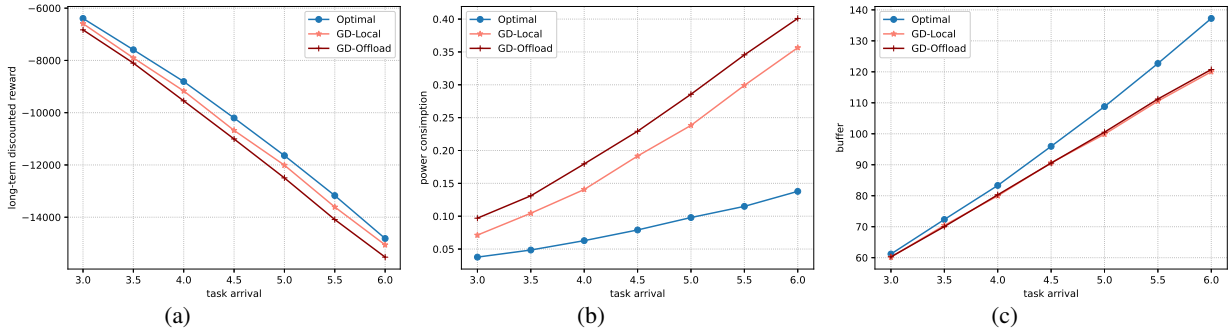


Fig. 9: Performance vs task arrival. (a) Long-term discounted reward; (b) Power consumption; (c) Buffer length.

has a slightly higher buffer length than other policies. This is because the objective of the optimal policy is to maximize the long-term discounted reward by making a tradeoff between power the consumption and buffer length, which may lead to the compromise for buffer length.

VII. CONCLUSIONS

In this paper, we considered the stochastic task arrival and uncertain channel condition caused by both the MIMO-NOMA channel interference and VU mobility in VEC, and proposed a decentralized power allocation scheme based on the DRL to maximize the long-term reward including the power consumption and delay. We first formulated the system model and then constructed a DRL framework where the state is defined as the local observations. The DDPG algorithm has been adopted to learn the optimal policy. Extensive simulations have demonstrated the optimal policy outperforms the other existing policies. According to the theoretical analysis and simulation results, the conclusions can be made as follows:

- Since the channel condition is impacted by the mobility of VU, more offloading power and less local execution power are consumed to process more tasks when the VU gets close to the BS. On the contrary, less offloading power and more local execution power are consumed when it gets far away from the BS.
- Compared with the signal-user scenario, the VU consumes more power to process more tasks under the optimal policy in the multi-user scenario due to the deteriorated channel caused by the interference among VUs.
- In order to maximize the long-term discounted reward, the optimal policy emphasizes the power consumption and compromises the buffer length as compared to the GD-Local and GD-Offload policies given different tasks arrival rates.

For the future work, we will consider the data freshness to design the offloading scheme in VEC.

REFERENCES

- [1] A. Bonadio, F. Chiti, and R. Fantacci, "Performance analysis of an edge computing saas system for mobile users," *IEEE Trans. Veh. Technol.*, vol. 69, no. 2, pp. 2049–2057, 2020.
- [2] Q. Wu, H. Liu, R. Wang, P. Fan, Q. Fan, and Z. Li, "Delay-sensitive task offloading in the 802.11p-based vehicular fog computing systems," *IEEE Internet of Things Journal*, vol. 7, no. 1, pp. 773–785, 2020.
- [3] Q. Wu, H. Ge, H. Liu, Q. Fan, Z. Li, and Z. Wang, "A task offloading scheme in vehicular fog and cloud computing system," *IEEE Access*, vol. 8, pp. 1173–1184, 2020.
- [4] X. Hou, Y. Li, M. Chen, D. Wu, D. Jin, and S. Chen, "Vehicular fog computing: A viewpoint of vehicles as the infrastructures," *IEEE Trans. Veh. Technol.*, pp. 3860–3873, 2016.
- [5] Q. Wu, S. Xia, P. Fan, F. Qiang, and Z. Li, "Velocity-adaptive v2i fair-access scheme based on ieee 802.11 dcf for platooning vehicles," *Sensors*, vol. 18, no. 12, pp. 4198–4198, 2018.
- [6] X. Liu, T. Huang, N. Shlezinger, Y. Liu, J. Zhou, and Y. C. Eldar, "Joint transmit beamforming for multiuser mimo communications and mimo radar," *IEEE Trans. Signal Process.*, vol. 68, pp. 3929–3944, 2020.
- [7] L. P. Qian, B. Shi, Y. Wu, B. Sun, and D. H. K. Tsang, "Noma-enabled mobile edge computing for internet of things via joint communication and computation resource allocations," *IEEE Internet of Things Journal*, vol. 7, no. 1, pp. 718–733, 2020.
- [8] T. L. Marzetta, "Noncooperative cellular wireless with unlimited numbers of base station antennas," *IEEE Trans. Wireless Commun.*, vol. 9, no. 11, pp. 3590–3600, 2010.
- [9] B. Di, L. Song, Y. Li, and Z. Han, "V2X meets noma: Non-orthogonal multiple access for 5g-enabled vehicular networks," *IEEE Wireless Commun. Mag.*, vol. 24, no. 6, pp. 14–21, 2017.
- [10] Q. Wu, H. Ge, P. Fan, J. Wang, Q. Fan, and Z. Li, "Time-dependent performance analysis of the 802.11p-based platooning communications under disturbance," *IEEE Transactions on Vehicular Technology*, vol. 69, no. 12, pp. 15760–15773, 2020.
- [11] J. Zheng and Q. Wu, "Performance modeling and analysis of the ieee 802.11p edca mechanism for vanet," *IEEE Transactions on Vehicular Technology*, vol. 65, no. 4, pp. 2673–2687, 2016.
- [12] M. Volodymyr, K. Koray, S. David, A. A. Rusu, V. Joel, M. G. Bellemare, G. Alex, R. Martin, A. K. Fidjeland, and O. Georg, "Human-level control through deep reinforcement learning," *Nature*, vol. 518, no. 7540, pp. 529–33, 2019.
- [13] W. Zhan, C. Luo, J. Wang, G. Min, and H. Duan, "Deep reinforcement learning based computation offloading in vehicular edge computing," in *2019 IEEE Global Communications Conference (GLOBECOM)*, 2019, pp. 1–6.
- [14] W. Zhan, C. Luo, J. Wang, C. Wang, G. Min, H. Duan, and Q. Zhu, "Deep-reinforcement-learning-based offloading scheduling for vehicular edge computing," *IEEE Internet of Things Journal*, vol. 7, no. 6, pp. 5449–5465, 2020.
- [15] H. Wang, H. Ke, G. Liu, and W. Sun, "Computation migration and resource allocation in heterogeneous vehicular networks: A deep reinforcement learning approach," *IEEE Access*, vol. 8, pp. 171140–171153, 2020.
- [16] P. Dong, Z. Ning, R. Ma, X. Wang, X. Hu, and B. Hu, "Noma-based energy-efficient task scheduling in vehicular edge computing networks: A self-imitation learning-based approach," *China Communications*, vol. 17, no. 11, pp. 1–11, 2020.
- [17] H. Ke, J. Wang, L. Deng, Y. Ge, and H. Wang, "Deep reinforcement learning-based adaptive computation offloading for mec in heterogeneous vehicular networks," *IEEE Trans. Veh. Technol.*, vol. 69, no. 7, pp. 7916–7929, 2020.
- [18] Y. He, N. Zhao, and H. Yin, "Integrated networking, caching, and computing for connected vehicles: A deep reinforcement learning approach," *IEEE Trans. Veh. Technol.*, vol. 67, no. 1, pp. 44–55, 2018.

- [19] L. T. Tan and R. Q. Hu, "Mobility-aware edge caching and computing in vehicle networks: A deep reinforcement learning," *IEEE Trans. Veh. Technol.*, vol. 67, no. 11, pp. 10 190–10 203, 2018.
- [20] Z. Ning, K. Zhang, X. Wang, M. S. Obaidat, L. Guo, X. Hu, B. Hu, Y. Guo, B. Sadoun, and R. Y. K. Kwok, "Joint computing and caching in 5g-envisioned internet of vehicles: A deep reinforcement learning-based traffic control system," *IEEE Trans. Intell. Transp. Syst.*, pp. 1–12, 2020.
- [21] Y. Liu, H. Yu, S. Xie, and Y. Zhang, "Deep reinforcement learning for offloading and resource allocation in vehicle edge computing and networks," *IEEE Trans. Veh. Technol.*, vol. 68, no. 11, pp. 11 158–11 168, 2019.
- [22] Q. Luo, C. Li, T. H. Luan, and W. Shi, "Collaborative data scheduling for vehicular edge computing via deep reinforcement learning," *IEEE Internet of Things Journal*, vol. 7, no. 10, pp. 9637–9650, 2020.
- [23] G. Qiao, S. Leng, S. Maharjan, Y. Zhang, and N. Ansari, "Deep reinforcement learning for cooperative content caching in vehicular edge computing and networks," *IEEE Internet of Things Journal*, vol. 7, no. 1, pp. 247–257, 2020.
- [24] Y. Ren, X. Yu, X. Chen, S. Guo, and Q. Xue-Song, "Vehicular network edge intelligent management : A deep deterministic policy gradient approach for service offloading decision," in *2020 International Wireless Communications and Mobile Computing (IWCMC)*, 2020, pp. 905–910.
- [25] H. Ye, G. Y. Li, and B. F. Juang, "Deep reinforcement learning based resource allocation for v2v communications," *IEEE Trans. Veh. Technol.*, vol. 68, no. 4, pp. 3163–3173, 2019.
- [26] Y. Xu, C. Yang, M. Hua, and W. Zhou, "Deep deterministic policy gradient (ddpg)-based resource allocation scheme for noma vehicular communications," *IEEE Access*, vol. 8, pp. 18 797–18 807, 2020.
- [27] F. Wang, J. Xu, and Z. Ding, "Optimized multiuser computation offloading with multi-antenna noma," in *2017 IEEE Globecom Workshops (GC Wkshps)*, 2017, pp. 1–7.
- [28] Y. Pan, M. Chen, Z. Yang, N. Huang, and M. Shikh-Bahaei, "Energy-efficient noma-based mobile edge computing offloading," *IEEE Commun. Lett.*, vol. 23, no. 2, pp. 310–313, 2019.
- [29] T. Huang, Y. Zhang, H. Wu, W. Jiang, C. Yao, M. Xu, and J. Feng, "Joint pilot and data transmission power control and computing resource allocation for the massive mimo based mec network," in *2019 IEEE 19th International Conference on Communication Technology (ICCT)*, 2019, pp. 860–865.
- [30] C. Ding, J. B. Wang, H. Zhang, M. Lin, and J. Wang, "Joint mu-mimo precoding and resource allocation for mobile-edge computing," *IEEE Trans. Wireless Commun.*, vol. 20, no. 3, pp. 1639–1654, 2021.
- [31] W. Feng, J. Zheng, and W. Jiang, "Joint pilot and data transmission power control and computing resource allocation algorithm for massive mimo-mec networks," *IEEE Access*, vol. 8, pp. 80 801–80 811, 2020.
- [32] Y. Jang, J. Na, S. Jeong, and J. Kang, "Energy-efficient task offloading for vehicular edge computing: Joint optimization of offloading and bit allocation," in *2020 IEEE 91st Vehicular Technology Conference (VTC2020-Spring)*, 2020, pp. 1–5.
- [33] H. Q. Ngo, E. G. Larsson, and T. L. Marzetta, "Energy and spectral efficiency of very large multiuser mimo systems," *IEEE Trans. Commun.*, vol. 61, no. 4, pp. 1436–1449, 2013.
- [34] Abramowitz and Milton, "Handbook of mathematical functions : with formulas, graphs and mathematical tables," *American Journal of Physics*, vol. 56, no. 10, pp. 958–962, 1988.
- [35] J. Kwak, Y. Kim, J. Lee, and S. Chong, "Dream: Dynamic resource and task allocation for energy minimization in mobile cloud systems," *IEEE J. Sel. Areas Commun.*, vol. 33, no. 12, pp. 2510–2523, 2015.
- [36] C. King, "Fundamentals of wireless communications," in *2014 IEEE-IAS/PCA Cement Industry Technical Conference*, 2014, pp. 1–7.
- [37] D. Silver, G. Lever, N. Heess, T. Degris, D. Wierstra, and M. Riedmiller, "Deterministic policy gradient algorithms," in *2014 International Conference on Machine Learning(ICML)*, 2014, pp. 387–395.

- [38] R. S. Sutton and A. G. Barto, "Reinforcement learning: An introduction," *IEEE Trans. Neural Netw.*, vol. 9, no. 5, pp. 51–52, 1998.
- [39] D. P. Kingma and J. Ba, "Adam: A method for stochastic optimization," *arXiv preprint arXiv:1412.6980*, vol. 9, 2015.
- [40] G. E. Uhlenbeck and L. S. Ornstein, "On the theory of the brownian motion," *Revista Latinoamericana De Microbiología*, vol. 15, no. 1, pp. 29–35, 1973.